International Journal of Biological Macromolecules 62 (2013) 629–635

Contents lists available at ScienceDirect

International Journal of Biological Macromolecules

journal homepage: www.elsevier.com/locate/ijbiomac

An amperometric hypoxanthine biosensor based on Au@FeNPs for determination of hypoxanthine in meat samples

Rooma Devi, Sujata Yadav, Renuka Nehra, C.S. Pundir*

Department of Biochemistry, Maharshi Dayanand University, Rohtak 124001, Haryana, India

ARTICLE INFO

Article history:
Received 17 July 2013
Received in revised form 7 October 2013
Accepted 8 October 2013
Available online 17 October 2013

Keywords:
Hypoxanthine biosensor
Boronic acid
Au@Fe nanomaterials
Meat
Pencil graphite

ABSTRACT

A xanthine oxidase (XOD) from buttermilk was immobilized covalently onto boronic acid functionalized gold coated iron nanoparticles (Au@FeNPs) electrodeposited on pencil graphite (PG) electrode, via the boroester linkages, between free hydroxyl groups of boronic acid, α-COOH and –NH_2 groups of enzyme. The surface functionalization of Fe/Au nanoparticles with boronic acid (Au@FeNPs) on pencil graphite (PG) electrode was characterized by Fourier transform infrared (FTIR), cyclic voltammetry (CV), scanning electron microscopy (SEM), atomic force microscopy (AFM) and Electrochemical impedance spectroscopy (EIS) before and after immobilization of XOD. The biosensor exhibited optimum response within 3 s at pH 7.2 and 30 °C and linearity in the range, 0.05 μM to 150 μM for hypoxanthine with a detection limit of 0.05 μM ($S/N = 3$). Apparent Michaelis Menten constant ($K_{m(app)}$) for hypoxanthine was 40 μM and I_{max} 0.125 mA. The biosensor was employed to determine hypoxanthine in fish, chicken, pork, beef meat and lost 50% of its initial activity after its 200 uses over 100 days, when stored at 4 °C.

1. Introduction

Hypoxanthine, (1*H*-purin-6(9*H*)-one) purine (Hx), is a derivative of adenine nucleotide, is accumulated in biological tissue, when it is stored at room temperature. The determination of Hx is very important for the quality control of fish products in food industries [1]. Various methods are available for determination of hypoxanthine such as colorimetric [2], fluorometric [3], HPLC [4], mass spectrometry [5], anion exchange chromatography, thin layer chromatography [6], mass fragmentography [7], capillary column gas chromatography [8], However, these methods require time consuming sample pretreatment, expensive and generally unportable equipment and trained person to operate. Therefore, there is an interest in developing a simple, sensitive, accurate, and portable system such as a biosensor for determination of hypoxanthine. The development of biosensors was driven by the need for faster and more versatile analytical methods for application in important areas such as clinical, biomedical, environmental, industrial, and pharmaceutical analysis [9]. The advantages of biosensors, relative to chromatographic techniques, are their fast response, cost effectiveness, and simplicity of operation and construction. A judicious choice of the biological receptor and applied potential improves their selectivity and sensitivity. Enzyme immobilization technology is an effective means to improve enzyme stability and perform its reuse [10,11].

Xanthine oxidase (EC 1.1.3.22) is molybdopterin-containing flavoprotein that catalyze the oxidation of hypoxanthine to xanthine and xanthine to uric acid with the reduction of molecular oxygen to water [12–18].

A number of hypoxanthine biosensors have been reported based on xanthine oxidase immobilized on various supports [19–21], but there are very few reports on its covalent immobilization. In recent years, the use of gold coating over magnetic nanoparticles (MNPs) for both biocompatible surface and the high magnetic properties has drawn intense scientific and technological interest for potential applications in bio-separation and bio-detection [22]. It is well recognized that gold layers with their excellent compatibility with biomolecules and non-toxic property provide not only the stability to the MNPs in solution, but also create a suitable surface for the binding of MNPs with various chemical and biological agents; which lead to expand the application scope of MNPs in various potential fields of bionanotechnology [23].

We described here in the surface functionalization of gold coated iron nanoparticles (Au@FeNPs) using boronic acid, which resulted into generation of several free hydroxyl functional groups on surface of Au@FeNPs. This property was used for covalent immobilization of xanthine oxidase on the surface of Au@FeNPs through boroester bonds and amide bond to construct an improved amperometric hypoxanthine biosensor.

* Corresponding author. Tel.: +91 1262 295480 O/+91 1262 272012 R/+91 9416492413; fax: +91 1262 295480.
E-mail addresses: pundircs@rediffmail.com, chandraspundir@gmail.com (C.S. Pundir).

0141-8130/$ – see front matter © 2013 Elsevier B.V. All rights reserved.
http://dx.doi.org/10.1016/j.ijbiomac.2013.10.009

2. Material and methods

2.1. Materials

4-Mercaptophenyl boronic acid, ferrous sulfate ($FeSO_4$), hydrogen tetrachloroaurate gold ($HAuCl_4$) (30% in dilute HCl), sodium borohydride ($NaBH_4$), cetyltrimethylammonium bromide ($C_{19}H_{42}BrN$) (CTAB), 1-butanol($(C_4H_{10}O$) and octane (C_8H_{18}) from Sigma-Aldrich USA, Xanthine oxidase (XOD) (E.C.1.1.3.2) from buttermilk (0.15 U/mg), hypoxanthine were from SRL, Mumbai, and All other chemicals were of AR grade.

2.2. Instruments

An Autolab Potentiostat/Galvanostat (Eco Chemie, Netherlands) was used with three electrode system consisting with XOD-Au@FeNPs/PG electrode as the working electrode, Ag/AgCl with saturated KCl as a reference electrode and platinum (Pt) wire as the counter electrode for amperometric study and electrochemical impedance spectroscopy (EIS) measurements. UV–visible spectra and FTIR spectra were recorded in UV–visible spectrophotometer (Shimadzu, Model 1700), FTIR spectrophotometer (Thermo Scientific, USA), respectively used. The morphological studies were carried out in transmission electron microscope (TEM) at Punjab University, Chandigarh, scanning electron microscope (SEM) (Model Joel JSM-6510, Japan), Atomic force microscopy (AFM) Nanoscope III scanning probe microscope (Digital Instruments, Santa Barbara, CA) at Department of Chemistry M.D. University Rohtak.

2.3. Construction of Au@FeNPs/PG electrode

2.3.1. Synthesis of Fe-core/Au-shell magnetic nanoparticles (Au@FeNPs)

Au@FeNPs were synthesized by reduction of $FeSO_4$ with $NaBH_4$ [24]. $FeSO_4$ (0.36 g) was mixed in reverse micelle solution (CTAB as the surfactant, co-surfactant of *n*-butanol and octane as the water phase) with 0.18 g of $NaBH_4$ stirred at room temperature. The solution turned green and then black, indicating the formation of Fe-NPs. After 1 h, 0.54 g of $HAuCl_4$ was added to the solution of Fe-NPs. Then, 0.22 g of $NaBH_4$ was added and solution was kept on stirring at room temperature for 12 h to form gold coated iron nanoparticles (Au@FeNPs). A dark solid was formed which, then separated by a magnet and washed with a chloroform/methanol (1:1) mixture. The product was then dried overnight in a vacuum oven, resulting into a black powder.

The morphology, particle size and structure of the Au@FeNPs were determined by a transmission electron microscopy (TEM) and UV spectroscopy.

2.3.2. Activation of Au@FeNPs with boronic acid

4-mercaptophenylboronic acid (10 g) was mixed with Au@FeNPs (6 g) in ethanol (100 ml). After vigorous stirring for 12 h at room temperature, the solvent was removed. Then, the dark residue was washed thoroughly with diethyl ether to remove excess 4-mercaptophenylboronic acid. Finally, the material was dried in vacuum oven at 40 °C to obtain the pure product as a dark solid.

2.3.3. Electrodeposition of Au@FeNPs on PG electrode

Prior to the surface modification, the pencil graphite (PG) electrode was cleaned with piranha solution [H_2SO_4:H_2O_2 in ratio 3:1 (v/v)] for 10 min and then rinsed thoroughly with distilled water. Au@FeNPs were electrochemically deposited onto PG electrode through cyclic voltammetry (CV) by applying 20 polymerization cycles at −0.6 V to +0.6 V as described [25] at a scan rate of 50 mV/s by immersing PG electrode in a solution (25 ml) containing 22 ml electrolyte [2.5 mM $K_3Fe(CN)_6/K_4Fe(CN)_6$ (1:1)] and 50 mg Au@FeNPs. The resulting Au@FeNPs/PG modified electrode was washed thoroughly with distilled water to remove unbound matter and kept in dry Petri plate at 4 °C.

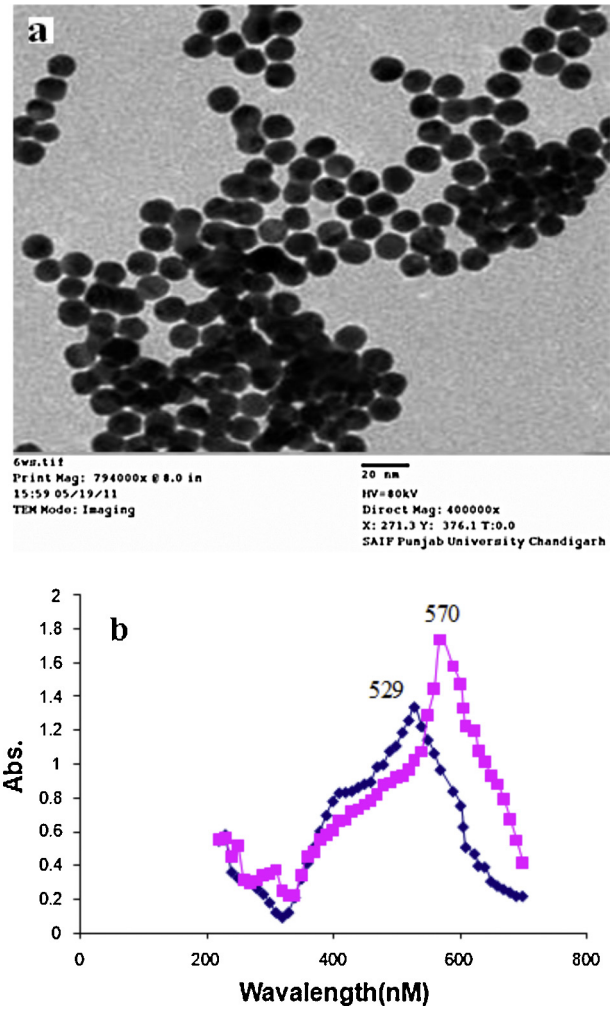

Fig. 1. (a) Transmission electron microscopic (TEM) images, of Au@FeNPs and (b) UV spectrum of Au and Au@FeNPs.

2.4. Immobilization of XOD onto Au@FeNPs/PG electrode

To immobilize XOD onto Au@FeNPs/PG electrode, the electrode was dipped into 10 μl solution of freshly prepared XOD containing 0.1Uand kept undisturbed for about 12 h at 4 °C. Finally, the electrode was immersed into 0.05 M sodium phosphate buffer (PBS) (pH 7.0) to wash out any unbound XOD from the electrode surface. The fabricated electrode was characterized by SEM, FTIR and EIS spectroscopy. Enzyme electrode was stored at 4 °C when not in use.

2.5. Cyclic voltammetric measurement and testing of hypoxanthine biosensor

Cyclic voltammogram (CV) of XOD- Au@FeNPs/PG electrode was recorded in potentiostat–galvanostat from −0.2 V to +0.6 V as described [20] at a scan rate of 50 mV/s by immersing PG electrode in a solution of electrolyte [2.5 mM $K_3Fe(CN)_6/K_4Fe(CN)_6$ (1:1)]. For amperometric studies, three electrodes were connected to a potentiostat/galvanostat and then immersed into 25 ml 0.05 M sodium

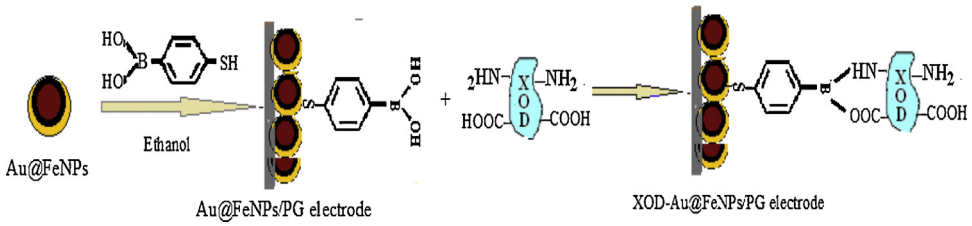

Fig. 2. Schematic representation of chemical reactions involved in fabrication of XOD-Au@FeNPs/PG electrode.

phosphate buffer (pH 7.2) in a 50 ml beaker. The reaction was started by adding hypoxanthine solution of different concentration in reaction mixture and the current (mA) generated was recorded at optimum voltage.

2.6. Optimization of hypoxanthine biosensor

To determine optimum pH, the pH was varied from 3.0 to 8.0 at an interval of 0.5. Similarly optimum temperature was studied by incubating the reaction mixture at different temperature (25–45 °C) and time. The effect of hypoxanthine concentration on biosensor response was determined by varying the concentration of hypoxanthine from 0.05 μM to 500 μM.

2.7. Amperometric determination of hypoxanthine in meat samples

Labeo fish purchased from a local market was chopped and homogenized in (5 ml 0.5 M $HClO_4$) until a fine paste was obtained. The denatured samples were mechanically stirred for 10 min and then centrifuged at 4000 rpm for 5 min. The supernatant was collected and its pH was adjusted to 7.0 with NaOH. The supernatant (fish meat extract) was diluted 10 times. Then these denatured sample solutions were divided into two parts. One part was used immediately and other was stored at room temperature. To determine hypoxanthine content in fish sample, same procedure was used as described for sensor's response measurement under the optimal working conditions except that hypoxanthine was

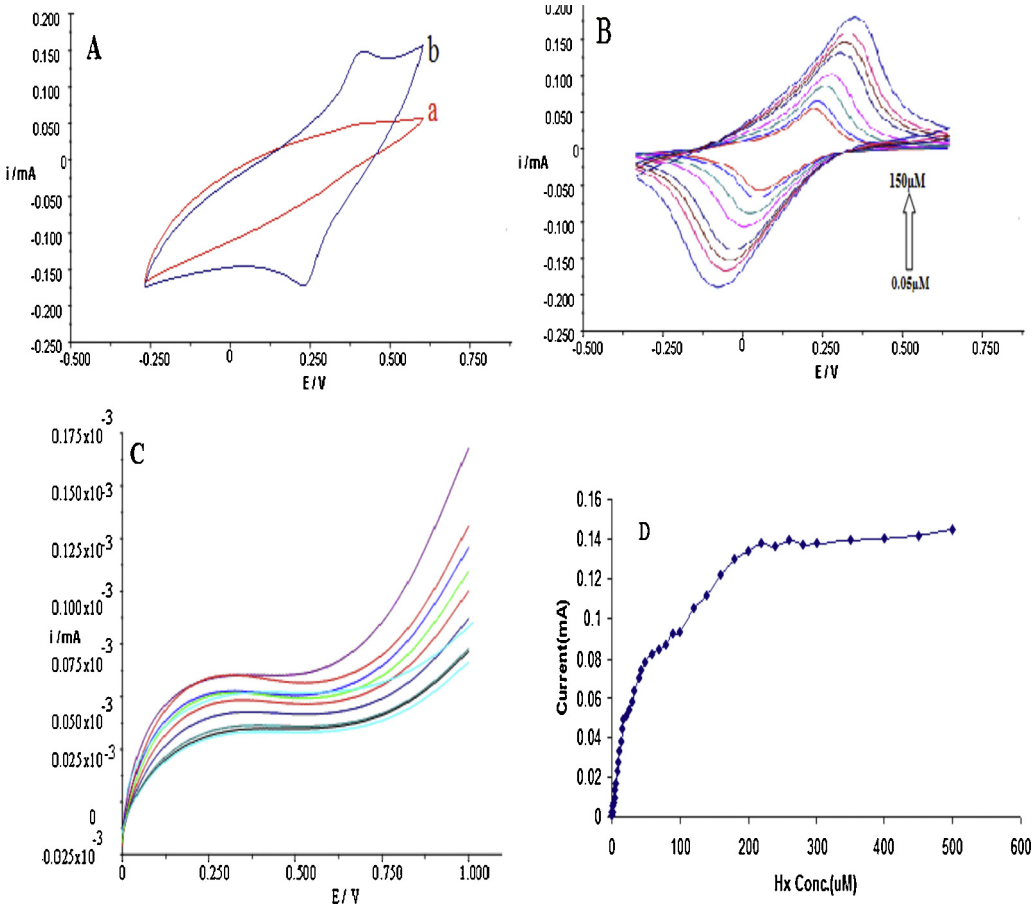

Fig. 3. (A) Cyclic voltammogram of bare PG electrode (a) and Au@FeNPs/PG electrode (b) (B) cyclic voltammetry of amperometric response studies of XOD-Au@FeNPs/PG electrode in hypoxanthine concentration from (0.05 μM to 150 μM) using sodium phosphate buffer (0.05 M, pH 7.2). (C) Linear sweep voltammetry in sodium phosphate buffer 0.05 M, pH 7.2, hypoxanthine (0.05 μM to 150 μM). (D) Effect of hypoxanthine concentration (0.05 μM to 150 μM) response of hypoxanthine biosensor based on XOD-Au@FeNPs/PG electrode.

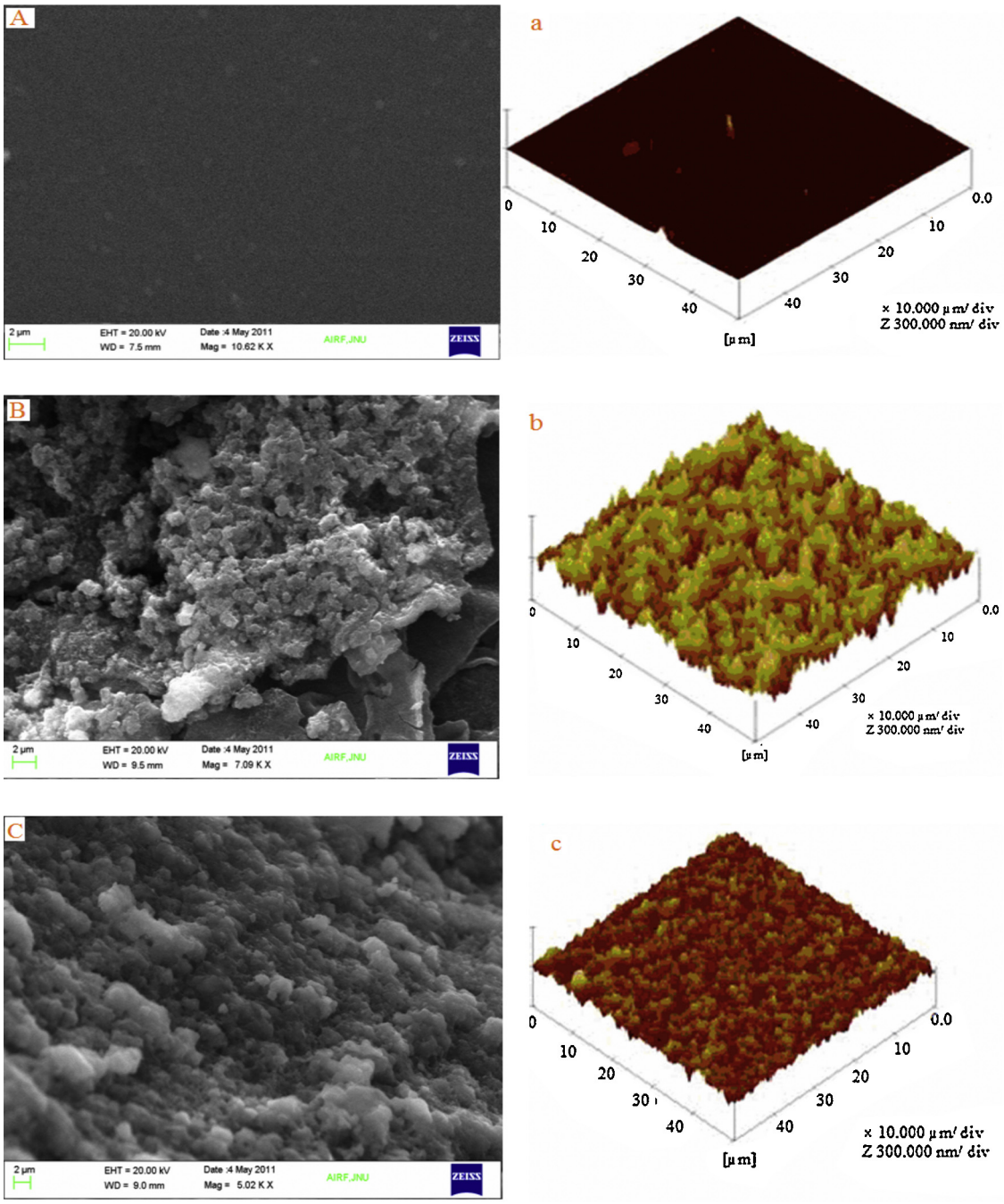

Fig. 4. SEM and AFM images of (A,a) Bare PG electrode (B,b) Au@FeNPs/PG electrode (C,c) XOD-Au@FeNPs/PG electrode.

replaced by the sample and the same processors was also followed for other meat sample (chicken, beef, pork) [13].

3. Results and discussion

3.1. Characterization of Au@FeNPs

The characterization of nanoparticles was carried out by UV spectrophotometric spectra and transmission electron microscopy (TEM) (Fig. 1). The morphology of Fe/Au nanoparticles was characterized by TEM analysis. Fig. 1(a) shows TEM images of core–shell Au@FeNPs. The size of iron core was about 16 nm, while the gold shell was about 3–5 nm and well coated on iron core. In addition, the gold shell was observed, as bright regions in outer layer of nanoparticles, while the core of iron appeared as dark regions in the center of nanoparticles. The Au@FeNPs were spherical with an average diameter around 20 nm and a remarkably narrow size distribution of the Au@FeNPs was observed. In Fig. 1(b) the absorption spectrum of Au@FeNPs was measured and compared with that of gold nanoparticles (AuNPs). The Au NPs had maximum absorption at 529 nm, while the Fe/Au colloid showed maximum at 570 nm [26,27].

3.2. Construction of Au@FeNPs/PG electrode and cyclic voltammetric measurement

Fig. 2 summarizes reaction involved in fabrication of the hypoxanthine biosensor based on immobilization of XOD onto

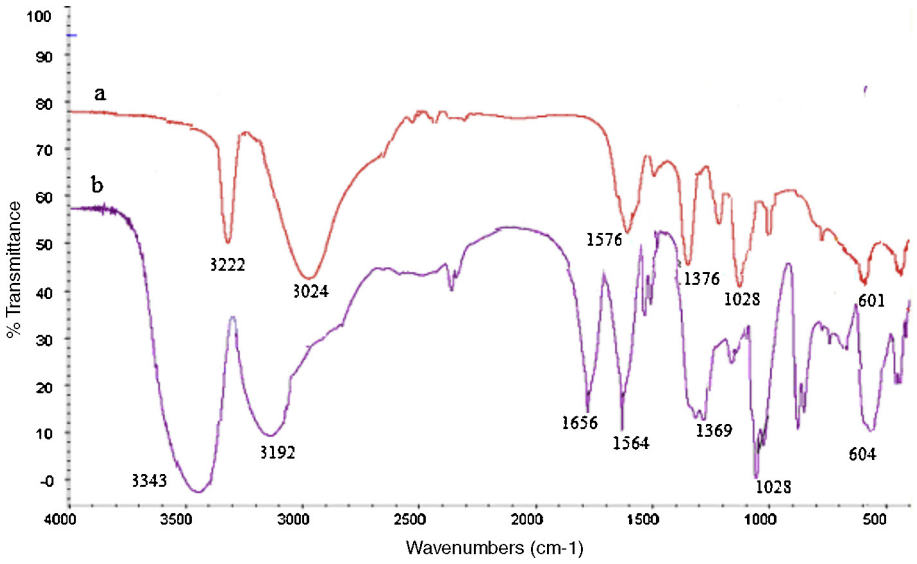

Fig. 5. FTIR spectra of (a) Au@FeNPs/PG electrode (b) XOD-Au@FeNPs/PG electrode.

Au@FeNPs/PG electrode. In order to evaluate the charge-transfer properties on the surface of the modified electrodes, cyclic voltammetry technique was employed, using $K_3Fe(CN)_6K_4Fe(CN)_6$ as redox probe. CV recorded in 2.5 mM $K_3Fe(CN)_6/K_4Fe(CN)_6$ solution and sodium phosphate buffer 0.05 M (pH 7.2) are shown in Fig. 3A. In bare PG electrode [curve (*a*), there is no oxidation and reduction peaks but after electrodeposition of Au@FeNPs on PG electrode [curve (*b*)] these was well defined oxidation and reduction peaks caused by Fe^{3+}/Fe^{2+} redox couples in forward and reverse scan. The electrodeposition of Au@FeNPs on PG electrode surface led to vast increase in current intensity as a result of the increase in electro active area. The preservation of a quasi reversible electrode process and the large increase in peak currents for the nanocomposite film modified electrode proved that Au@FeNPs exerted an obvious improvement effect on electric conductivity of enzyme electrode. In Fig. 3B shows CV of XOD-Au@FeNPs/PG electrode in presence of different hypoxanthine concentration. The oxidation peak seen at 0.4 V corresponding to the oxidation of H_2O_2 arisen due to the enzymatic reaction between xanthine oxidase and hypoxanthine. The increase in the value of the oxidation current with increase in hypoxanthine concentration resulted due to the increased concentration of H_2O_2 during enzymatic reaction. The linear sweep voltammetry corresponding to the modified electrode is shown in Fig. 3C, of amperometric response studies of as a function of XOD- Au@FeNPs/PG electrode in concentration from (0.05 μM to 150 μM) using phosphate buffer (50 mM, pH 7.2). The response of the present electrode system in relation to the change in hypoxanthine concentration was linear in the range 0.05 μM to 500 μM) (Fig. 3D).

3.3. Surface morphological characterizations using SEM and AFM studies

The morphology of PG electrode, Au@FeNPs/PG electrode and XOD immobilized onto Au@FeNPs/PG electrode was characterized by SEM studies and AFM studies. The SEM and AFM images of the PG electrode showed a smooth and featureless morphology, (Fig. 4A,a) whereas nanocomposite displayed a layering and granular morphology attributed to the dispersion of Au@FeNPs and AFM image of gold coated iron nanoparticles in the size range of 40 × 40 nm were uniformly distributed throughout the film surface (Fig. 4B,b) were covered by spherical nature of multiparticles, presumably because of weak interactions and immobilization of XOD onto the Pencil graphite electrode shows a globular structure of enzyme(Fig. 4C,c).

3.4. FTIR spectra

The FTIR spectra of Au@FeNPs are shown in Fig. 5a. The peaks at 3024 cm^{-1}, 1576 cm^{-1}, and 1028 cm^{-1} could be assigned to the presence of aromatic ring, while aryl-boroxine bonds typically displayed a band at 1376 cm^{-1}. Furthermore, a board band at 3222 cm^{-1} indicates the presence of free hydroxyl functional groups of boronic acid on the sample. These results confirmed that the surface of Au@FeNPs was successfully functionalized by 4-mercaptophenylboronic acid. After the binding process of Au@FeNPs with XOD, significant changes were observed in the IR spectrum. As can be seen from Fig. 5b, new peaks at 3343 cm^{-1} and 3192 cm^{-1} arose, which could be assigned to the N–H stretching band, while a new strong peak at 1656 cm^{-1} can be attributed to the N–H bending band of the primary amine group in XOD with nanoparticles. It can also be noted that the strong peaks at around 1368 cm^{-1} and 604 cm^{-1} were assigned to B–O stretching band and B–O bending band, respectively, while peak at 1574 cm^{-1} was in correspondence with the characteristic absorption of aryl group, which confirmed that XOD was immobilized onto surface of Au@FeNPs working electrode via boroester linkages or amide bond [28].

3.5. Electrochemical impedance measurements

Fig. 6 shows electrochemical impedance spectra (EIS) of (A) PG electrode, (B) Au@FeNPs/PG and (C) XOD-Au@FeNPs/PG electrode, respectively. The charge transfer process in XOD-Au@FeNPs/PG electrode was studied by monitoring charge transfer resistance (R_{CT}) at the electrode and electrolyte interface. The value of the electron transfer resistance (semicircle diameter) (R_{CT}) depends on the dielectric and insulating features at the electrode/electrolyte interface. The increased R_{CT} value of XOD-Au@FeNPs/PG electrode was due to the immobilization of XOD onto Au@FeNPs/PG surface. The electron transfer via redox couple was hindered by the presence of xanthine oxidase on the electrode surface.

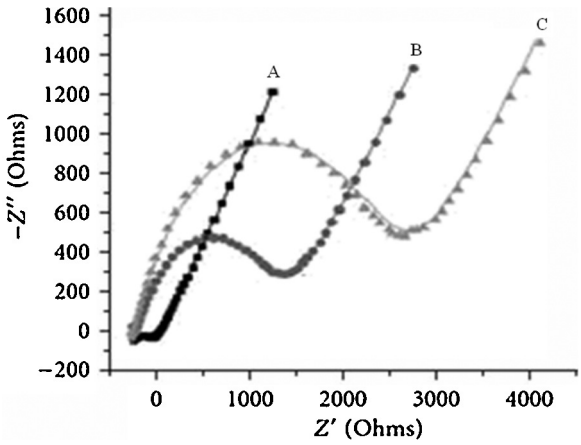

Fig. 6. Impedance spectra of (A) bare PG electrode, (B) Au@FeNPs/PG and (C) XOD-Au@FeNPs/PG electrode in sodium phosphate buffer (0.05 M, pH 7.2) containing $[K_3Fe(CN)_6/K_4Fe(CN)_6]$ (5 mM).

3.6. Optimization of experimental conditions of biosensors

The optimum current response of biosensor was obtained at pH 7.2(Fig. 7A) and 30 °C (Fig. 7B). When hypoxanthine was added into sodium phosphate buffer, pH 7.2 the biosensor responded rapidly to the substrate and achieved 95% of steady current less than in 3 s (Fig. 7C). This faster response could attribute due to the influence of nanoparticles (Au@FeNPs). The steady state amperometric response of biosensor was investigated by increasing hypoxanthine concentration from 0.05 μM to 150 μM under optimal conditions. The resulted calibration plot for hypoxanthine was linear over the concentration range 0.05 μM to 150 μM at optimum voltage 0.4 V (Fig. 7D). Lineweaver–Burk plot gave apparent $K_{m(app)}$ value of 40 μM and I_{max} 0.125 mA for immobilized xanthine oxidase.

3.7. Evaluation of biosensor

There was a linear relationship between current and hypoxanthine concentration ranging from 0.05 μM to 150 μM in reaction mixture. The detection limit ($S/N = 3$) of the present electrode system was 0.05 μM. To study analytical recovery, exogenous hypoxanthine of known concentration was added to the fish meat sample. The concentration of hypoxanthine was measured in fish meat sample before and after addition of exogenous hypoxanthine. The % recovery of added hypoxanthine in fish meat sample was calculated. Analytical recovery of added hypoxanthine in fish meat sample (10 mg/l and 20 mg/l) in % was 96.6% and 97.4%, respectively, indicating good efficiency of the biosensor. The within and between batch coefficient of variation for hypoxanthine determination in meat sample by the present biosensor were 2.76% and 2.95%, respectively, revealing the reproducibility and reliability of the method. The accuracy of the present method was tested by comparing hypoxanthine values (in %) in 10 meat samples by the present method (y) with those obtained by standard enzymic colorimetric method (x). The values obtained by both methods showed a very good correlation with $r = 0.99$.These results indicate a very good analytical performance of the present biosensor in biological samples.

3.7.1. Effect of interfering compounds

The ability of the immobilized enzyme layer to protect the sensor from electroactive interference was investigated. Other coexisting substances found in meat sample were studied for any possible interfering effect on analysis of hypoxanthine in meat

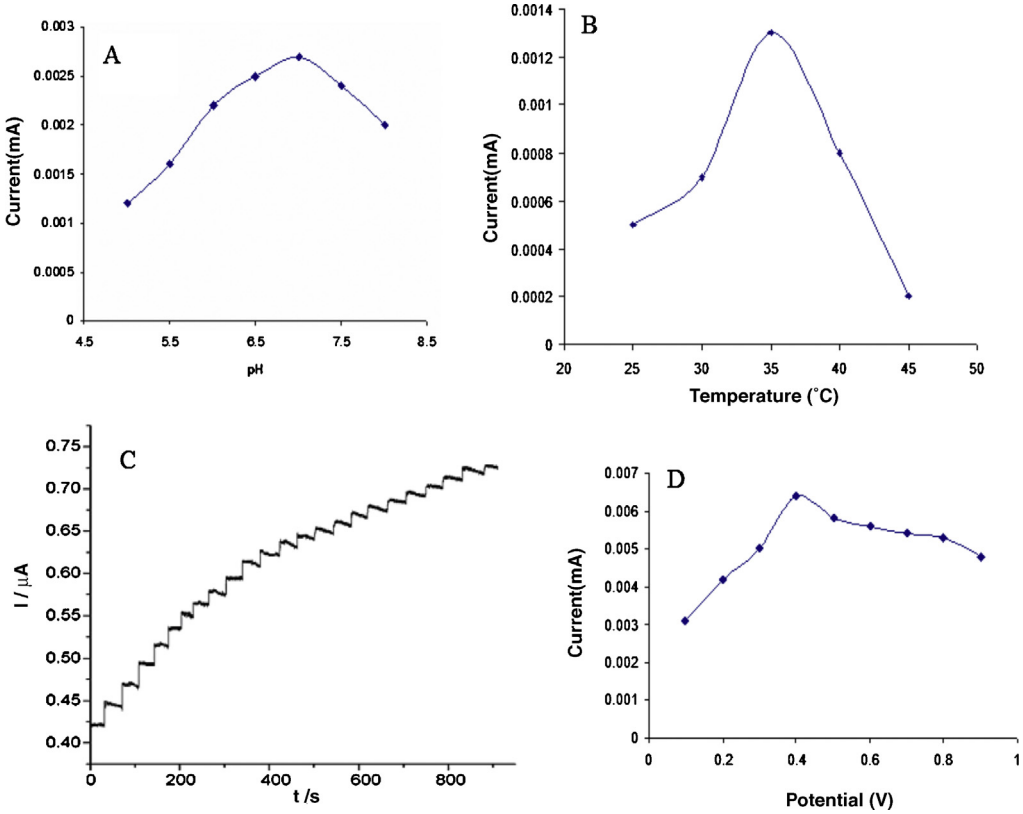

Fig. 7. (A) Effect of pH on response of hypoxanthine biosensor based on Au@FeNPs/PG electrode bound xanthine oxidase, (B) effect of incubation temperature on response of hypoxanthine biosensor based on Au@FeNPs/PG electrode bound xanthine oxidase, (C) current–time responses curve of XOD-Au@FeNPs/PG electrode, (D) voltage study for XOD-Au@FeNPs/PG electrode (0.15 mM hypoxanthine, 0.05 M sodium phosphate buffer solution, pH 7.2).

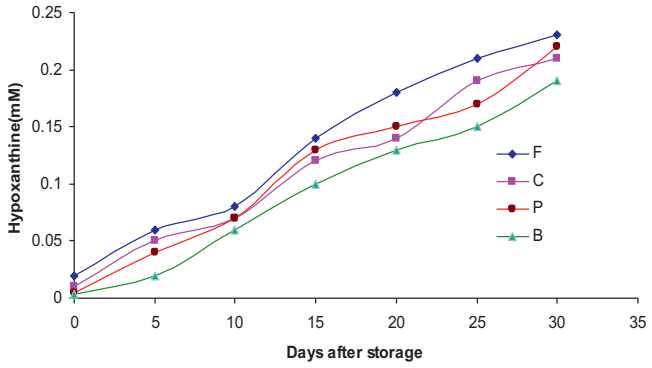

Fig. 8. Determination of hypoxanthine in fish (F), chicken (C), beef (B)and pork (P). Hypoxanthine biosensor based on XOD-Au@FeNPs/PG electrode during storage at room temperature (30 ± 5 °C).

sample. Known concentration (40 μM) of inosine 5-phospahate (IMP), inosine, cystine, uric acid, caffeine, theophylline and ascorbic acid were also added to 0.15 mM hypoxanthine solution. It was observed individually that of inosine 5-phospahate (IMP), inosine, cystine caffeine, theophylline, ascorbic acid and uric acid had practically no interfering effects on analysis of hypoxanthine.

3.7.2. Determination of hypoxanthine in meat

The hypoxanthine concentration in different meat sample was determined by the present biosensor at different storage time ranging from 1 to 30 days at room temperature. Hypoxanthine level was increased as the storage time was increased (Fig. 8).

3.8. Storage stability of enzyme electrode

The biosensor lost 50% of its initial activity during its regular use for 200 times over a period of 100 days when stored in 0.05 M sodium phosphate buffer, pH 7.2 at 4 °C, which is much better than earlier electrodes [19,28].

4. Conclusion

An amperometric biosensor for determination of hypoxanthine has been developed based on boronic acid functionalized gold coated iron nanoparticles (Au@FeNPs). Due to boronic acid attached onto the gold layer, the covalent immobilization of xanthine oxidase onto the surface of Fe/Au nanoparticles was obtained through the formation of boroester and amide bonds. The use of Au@FeNPs for construction of amperometric hypoxanthine biosensor has resulted into relatively rapid response, higher sensitivity, broad linear range, lower detection limit, good reproducibility and long term stability of the biosensor.

References

[1] C.S. Bavarsco, A.T. Zugno, B. Tagliar, C.M.D. Wannmacher, M. Wajner, A.T.S. Wyse, Int. J. Dev. Neurosci. 22 (2004) 11–17.
[2] G. Berti, P. Fossati, G. Tarenghi, C. Musitelli, G.V. Melzideril, J. Clin. Chem. Clin. Biochem. 26 (1988) 399–404.
[3] J.S. Beckman, D.A. Parks, J.D. Pearson, P.A. Marshall, B.A. Freeman, Free Radical Biol. Med. 6 (1989) 607–615.
[4] R. Kock, B. Delvoux, H. Gresiling, J. Clin. Chem. Clin. Biochem. 31 (1993) 303–310.
[5] R. Prker, W. Snedden, R.W. Watts, Biochem. J. 115 (1969) 103–108.
[6] H.S. Nakatani, L.V.D. Santos, C.P. Pelegrine, M. Gomes, M. Matsushita, N.E.D. Souza, J.V. Visentainer, Am. J. Biochem. Biotech. 1 (2005) 85–89.
[7] R.O. Olojoa, R.H. Xiab, J.J. Abramsona, Anal. Biochem. 339 (2005) 338–344.
[8] S. Renata, L. Pagliarussi, A.P. Luís, L. Freitas, J.K. Bastos, J. Sep. Sci. 25 (2002) 371–374.
[9] J.H.T. Luong, K.B. Male, J.D. Glennon, Biotechnol. Adv. 26 (2008) 492–500.
[10] S. Hu, C. Xu, J. Luo, D. Cui, Anal. Chim. Acta 412 (2000) 55–61.
[11] X.H. Li, Z.H. Xie, H. Min, Y.Z. Xian, L. Tongjin, Anal. Lett. 41 (2008) 456–468.
[12] J. Zhao, J.P. O'Daly, R.W. Henkens, Biosens. Bioelectron. 11 (1996) 493–502.
[13] R. Devi, M. Thakur, C.S. Pundir, Biosens. Bioelectron. 26 (2011) 3420–3426.
[14] R. Devi, S. Yadav, C.S. Pundir, Biochem. Eng. J. 58 (2011) 148–153.
[15] R. Devi, S. Yadav, C.S. Pundir, Colloids Surf., A 394 (2012) 38–45.
[16] R. Devi, S. Yadav, C.S. Pundir, Analyst 137 (2012) 754–759.
[17] R. Devi, J. Narang, S. Yadav, C.S. Pundir, J. Anal. Chem. 67 (2010) 273–277.
[18] C.S. Pundir, R. Devi, J. Narang, S. Singh, J. Nehra, S. Chaudhry, J. Food Biochem. 36 (2011) 21–27.
[19] L.Agui J.Y. Manso, P. Yanez-Sedeno, J.M. Pingarron, Sens. Actuators, B 133 (2006) 272–280.
[20] L. Mao, F. Xu, Q. Xu, L. Jin, Anal. Biochem. 292 (2001) 94–101.
[21] A.K. Basu, P. Chattopadhyay, U. RoyChoudhury, R. Chakraborty, Indian J. Exp. Biol. 43 (2005) 646–653.
[22] H.Y. Park, M.J. Schadt, L. Wang, I.-Im.S. Lim, P.N. Njoki, S.H. Kim, M.Y. Jang, Luo J., C.J. Zhong, Langmuir 23 (2007) 9050–9056.
[23] W. Hui, F. Shi, K. Yan, M. Peng, X. Cheng, Y. Luo, X. Chen, V.A.L. Roy, Y. Cui, Z. Wang, Nanoscale 4 (2012) 747–751.
[24] T.A. Pham, N.A. Kumar, Y.T. Jeong, Colloids Surf., A 370 (2010) 95–101.
[25] Y. Zhang, G.M. Zeng, L. Tang, D.L. Huang, X.Y. Jiang, Y.N. Chen, Biosens. Bioelectron. 22 (2007) 2121–2126.
[26] J. Lin, W. Zhou, A. Kumbhar, J. Weimann, J. Fang, E.F. Carpenter, J. Solid State Chem. 159 (2001) 26–31.
[27] L. Rivas, S. Sanchez-Cortes, J.V. García-Ramos, G. Morrcillo, Langmuir 16 (2000) 9722–9728.
[28] S. Hu, C.C. Liu, Electroanalysis 9 (1997) 372–377.